https://doi.org/10.1016/j.jpowsour.2019.02.097

A high-performance Zn battery based on self-assembled nanostructured $NiCo_2O_4$ electrode

Wenxu Shang[1], Wentao Yu[1], Peng Tan[1,2,*], Bin Chen[2], Haoran Xu[2], Meng Ni[2,3,*]

1 Department of Thermal Science and Energy Engineering, University of Science and Technology of China, Hefei 230026, Anhui, China
2 Department of Building and Real Estate, The Hong Kong Polytechnic University, Hung Hom, Kowloon, Hong Kong, China
3 Environmental Energy Research Group, Research Institute for Sustainable Urban Development (RISUD), The Hong Kong Polytechnic University, Hung Hom, Kowloon, Hong Kong, China

*Corresponding author.
E-mail addresses: pengtan@ustc.edu.cn (Peng Tan), meng.ni@polyu.edu.hk (Meng Ni)

Abstract:

Zn batteries are attractive for energy storage due to their low cost and intrinsic safety. However, the low utilization of active materials results in unsatisfied capacities. Herein, Zn batteries based on nanostructured $NiCo_2O_4$ electrodes are developed. Through hydrothermal reactions, porous $NiCo_2O_4$ nanosheets, nanowires, and nanoplates are fabricated, which are in-situ grown on the surface of nickel foam substrates and facilitate the electron transport and electrochemical reactions. In particular, the battery with the nanowire electrode exhibits the largest discharge capacity of 230.1 mAh g^{-1}, which accounts for 68.7% of the theoretical capacity of $NiCo_2O_4$. Based on the weights of $NiCo_2O_4$ and consumed Zn, the energy density of the battery is 301.3 Wh kg^{-1}, higher than most of the reported Zn batteries. At a current density of 8 A g^{-1}, the capacity is still 164.25 mAh g^{-1}, with the retention of 71.38%, which illustrates the high rate performance. Moreover, after 1000 discharge-charge cycles, the capacity retention is 63.23%, which reveals remarkable

cycling stability. The results show that the $NiCo_2O_4$ nanowire electrode is attractive for Zn batteries with high capacity, energy density, rate performance, and cycling stability.

Keywords: Zinc battery; Morphology; Nanostructured; Transition metal oxide; Electrochemical performance.

Highlights

- Nanostructured $NiCo_2O_4$ is in-situ grown on the nickel foam substrate.
- The $NiCo_2O_4$ nanowire electrode exhibits the best electrochemical performance.
- A Zn battery delivers the energy density of 301.3 Wh kg^{-1}.
- 71.38% of the capacity is preserved when the current increases from 0.5 to 8 A g^{-1}.
- The capacity retention researches 63.23% after 1000 discharge-charge cycles.

1. Introduction

With the fast-growing demands for portable electronic devices, it is urgent to develop battery systems with high capacities and low prices. As one of the most promising battery systems for energy storage, lithium-ion batteries have been commercially used around our life owing to the remarkable energy densities, high energy efficiency, and long cycle life [1,2]. However, lithium-ion batteries suffer from various issues for further applications, including the high price, safety problems, and insufficient capacity [3]. Therefore, exploring new battery systems with low price, intrinsic safety, and high capacity is in great need [4,5].

Among various alternative batteries, zinc-based batteries have got increasing

research attention in recent years [6–11]. Based on the metallic zinc, the theoretic capacity can research 825 mAh g_{zn}^{-1} [12], and the price is low (~2500 dollars per ton) [13]. Besides, aqueous electrolytes instead of organic ones can be used, resulting in high safety [14]. Till now, various kinds of Zn batteries have been developed, such as Zn-MnO_2 [15], Zn-Ni [16], and Zn-Ag batteries [17]. Although based on different electrode materials, the operating mechanisms during discharge and charge are similar, which involve the oxidation and reduction of zinc on the negative electrode and another redox couple of transition metals on the positive electrode [18]. However, although a high working voltage of 1.75 V can be delivered, the energy density is limited to the positive electrode (e.g., 228 Wh kg^{-1} based on NiO for Zn-Ni battery) [19]. Hence, tremendous efforts have been devoted to exploring new positive electrode materials with higher capacities to improve the energy densities of the batteries [20].

Cobalt, as one kind of transition metals, has been applied in the form of cobalt oxide (Co_3O_4) in Zn-based batteries recently. Wang et al. reported ultrathin porous Co_3O_4 nanosheets as the active electrode for a Zn-Co battery [14]. It exhibited a high discharge voltage of 1.78 V, a high energy density of 241 Wh kg^{-1}, and high capacity retention of 80% after 2000 cycles. Ma et al. reported a highly reversible Zn/Co^{3+} rich-Co_3O_4 battery, which worked well in a mild aqueous electrolyte solution (2 M $ZnSO_4$ + 0.2 M $CoSO_4$) and demonstrated a high average voltage of ~2.2 V, high specific capacity of 205 mAh g^{-1} at 0.5 A g^{-1}, and long cycling performance (~5000 cycles with a capacity retention of 92%) [9]. In our previous work, a nickel

foam-based electrode made of Co_3O_4 nanowire-assembled clusters was fabricated, which showed a discharge capacity of 173.6 mAh g^{-1} at 1 A g^{-1} [10]. However, the reported capacities are still lower than the theoretical capacity of Co_3O_4 (446 mAh g^{-1}) [14], resulting in a low utilization ratio of the active material (<50%).

The electrochemical performance of the active material inside the battery is closely related to the electron and ion transport [21]. Previous research has indicated that using element doping can enhance electron transport. Based on the site preference theory [22], the partial substitution of transition metals (i.e., Mn, Ni, and Cu) for Co in the Co_3O_4 lattice can get an inverse spinel structure [23–25], which delivers 3D networks of the interconnected interstitial space, achieving high electrical conductivity and ion diffusivity [26]. For example, Liu et al. reported that Co_3O_4 can produce an additional electron in the 3d orbital by the substitution of Co^{2+} by Ni^{2+}, which can modulate the electronic structure effectively. Consequently, the specific capacitance of a supercapacitor with $NiCo_2O_4$ can reach 1828 F g^{-1}, much higher than that with Co_3O_4 (948 F g^{-1}) [21,27]. In addition, the morphology of the electrode material can change the specific surface area and the contact interfaces with the electrolyte, affecting the ion transport [28]. For instance, He et al. reported that Co_3O_4 nanowire has the obvious bimodal pore structure with dominant macropores and small mesopores, delivering larger specific area (99.783 m^2 g^{-1}) than nanosheet (75.295 m^2 g^{-1}) [29]. Our finding also indicated that the nanowire-assembled clustered Co_3O_4 could deliver a higher capacity than that of previous work with nanosheet-liked Co_3O_4 [10]. Even with these progress on the electrodes, however, a high-capacity Zn battery

with high utilization of the active material has not been reported yet.

To this end, the aim of this work is to develop a high-performance Zn battery based on spinel cobalt materials. Based on the previous work that partially substitution of Co^{2+} by Ni^{2+} can lead to the superior electrochemical properties [27], we used $NiCo_2O_4$ as the active material in the battery. First, different morphologies of nanostructured $NiCo_2O_4$ in-situ grown on the nickel foam substrate were fabricated, and the properties were characterized. Then, their electrochemical performance as positive electrodes was examined in Zn batteries, from which the one with the largest capacity was selected. Further, a Zn battery was built based on the selected $NiCo_2O_4$ electrode, and the electrochemical performance, including the capacity, rate performance, coulombic efficiency, and cycling stability, was carefully evaluated.

2. Experimental

2.1 Synthesis of nanostructured $NiCo_2O_4$

The nanostructured $NiCo_2O_4$ with different morphologies on the nickel foam substitute was fabricated through hydrothermal reactions [10]. Briefly, nickel foam was first cleaned by dilute HCl solution, and then washed with distilled water and dried thoroughly. 40 mL of a homogeneous aqueous solution composed of 0.2 g of $Co(NO_3)_2 \cdot 6H_2O$, 0.4 g of $Co(NO_3)_2 \cdot 6H_2O$, 0.3 g of NH_4F, and 0.6 g of $CO(NH_2)_2$ was transferred into a Teflon-lined stainless-steel autoclave, and a piece of prepared nickel foam with a given surface area was immersed. To produce different morphologies, the sealed autoclaves were maintained at different temperatures (80, 120, and 160 °C) for 9 h. After cooled down naturally, the nickel foam with precursors was taken out, rinsed

carefully, and calcined at 250 °C in air for 3 h using a heating rate of 1 °C min^{-1} to convert the precursor to $NiCo_2O_4$. The loading of $NiCo_2O_4$ formed at different hydrothermal temperatures was controlled to be around 1.2 mg cm^{-2}.

2.2 Physicochemical characterization

The morphologies of the samples were observed by a scanning electron microscope (SEM, VEGA3 TESCAN) at 20 kV. The compositions were analyzed by X-ray diffraction (XRD, Rigaku Smartlab) using a Cu-Kα source at 45 keV. The formed nanostructures were examined by a transmission electron microscope (TEM, JEOL 2100F) at 200 kV. The specific surface area and pore volume were calculated by the Brunaure-Emmert-Teller (BET) and Barrett-Joyner-Halenda (BJH) methods, respectively, which were got from the nitrogen adsorption-desorption isotherms measured by ASAP 2020. The valences of Ni and Co of the samples were analyzed by the X-ray photoelectron spectroscopy (XPS, PHI 5600 multi-technique system) using Al monochromatic X-ray at 350 W.

2.3 Battery fabrication and evaluation

A Zn battery was fabricated using the nanostructured $NiCo_2O_4$ on the nickel foam as the positive electrode and a Zn plate as the negative electrodes, and an electrolyte composed of 6 M KOH and 0.1 M zinc acetate. The discharge and charge capacities were tested under different current densities based on the loading of $NiCo_2O_4$ in the voltage range of 1.4–1.9 V. The rate performance was measured at various current densities from 0.5 to 8 A g^{-1}, and the cycling stability test was carried out at 1 A g^{-1} in the same voltage range.

3. Results and discussion

3.1 Characterization of nanostructured $NiCo_2O_4$

The SEM images of the samples treated with different hydrothermal reaction temperatures are shown in Fig. 1. Using the hydrothermal temperature of 80 ^oC results in the nanosheet morphology (Fig. 1a). From Figs. 1a and S1a, nanosheets with the thickness of ~10 nm and the height of ~5.3 μm are grown perpendicularly on the nickel form surface and interconnected with each other. When the hydrothermal temperature increases to 120 ^oC, the morphology changes to nanowire (Figs. 1c and 1d). As the high-magnification image shown in Fig. 1d, the nanowires with an average length of 5.7 μm (Fig. S1b) are uniformly coated on the nickel foam surface. In addition, the tips of the nanowires are gathered, which may improve the structural stability and the utilization of the active material. Further increasing the hydrothermal temperature to 160 ^oC, interestingly, condensed nanoplates are accumulated on the surface, as shown in Figs. 1e and 1f. From Fig. S1c, the height of the nanoplates was measured to be 2.1 μm. Thus, different hydrothermal temperatures greatly change the morphologies of the active material.

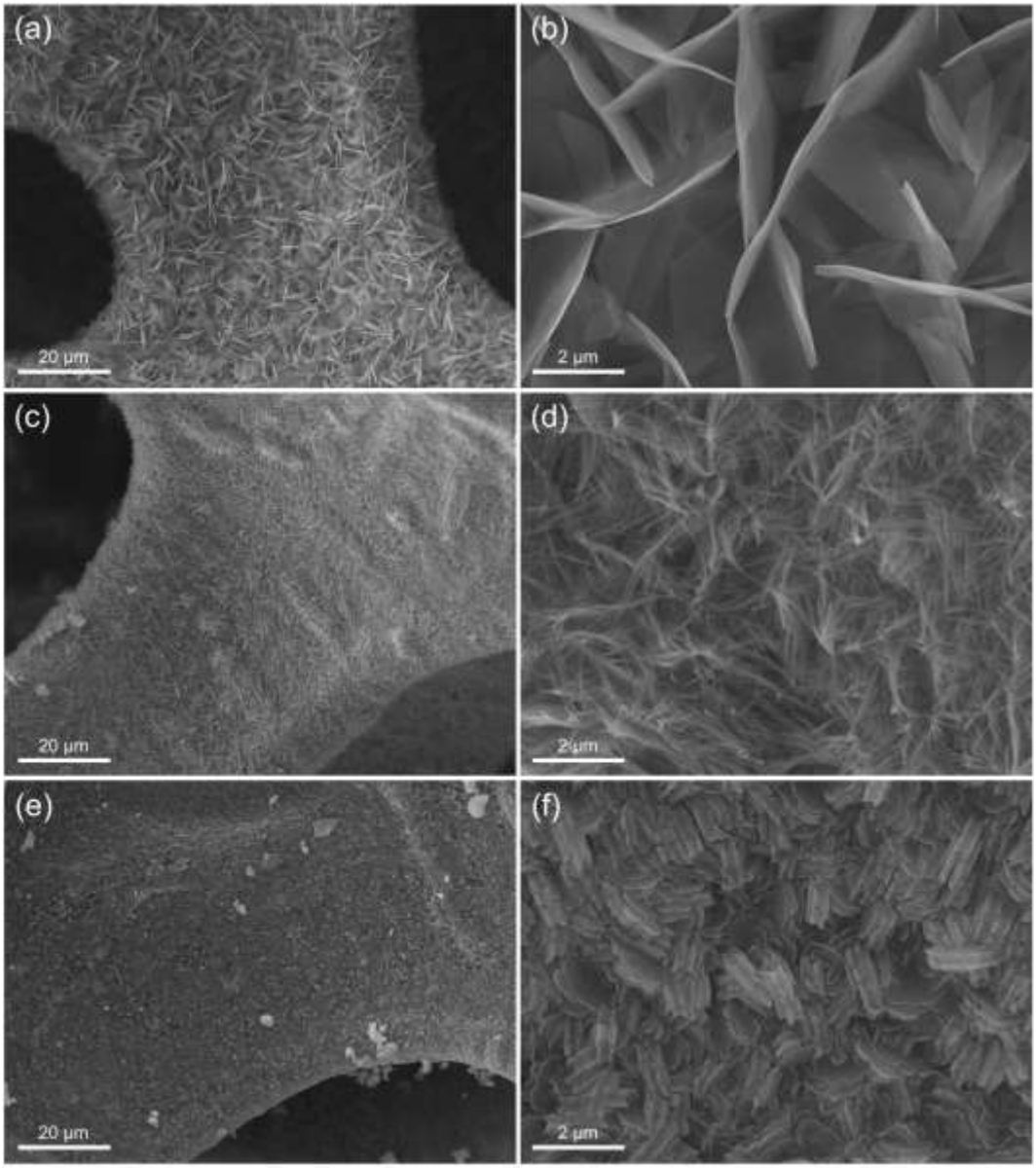

Fig. 1 SEM images of the nanostructured $NiCo_2O_4$/Ni foam from different hydrothermal reaction temperatures. (a-b) 80 ^oC, (c-d) 120 ^oC, and (e-f) 160 ^oC.

The XRD patterns of the synthesized samples are displayed in Fig. 2. In addition to the two diffraction peaks of the Ni substrate, the peaks at 18.93^o, 31.15^o, 36.70^o, 38.40^o, 59.11^o, and 64.96^o can be perfectly indexed to the (111), (220), (311), (222) (511), and (440) planes of spinel $NiCo_2O_4$ (PDF #73-1702), respectively. The results demonstrate that through using different hydrothermal reaction temperatures, nanostructured $NiCo_2O_4$ with different morphologies have been successfully

synthesized, which are in-situ gown on the surface of the nickel foam substrate without binders.

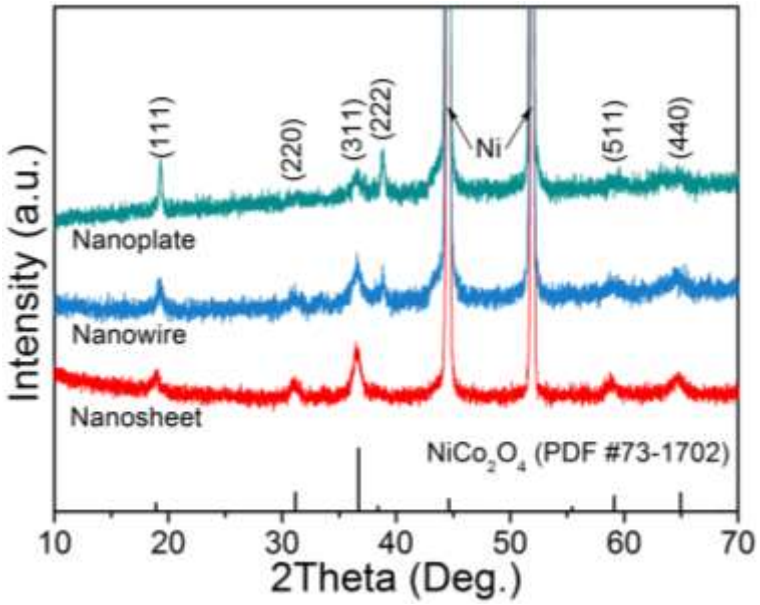

Fig. 2 XRD patterns of nanostructured $NiCo_2O_4$ with different morphologies.

The microstructures of $NiCo_2O_4$ with different morphologies were characterized by TEM. From Fig. 3, the nanostructured $NiCo_2O_4$ was assembled by a large number of interconnected nanoparticles and showed polycrystalline properties, as demonstrated in the selected area electron diffraction (SAED) patterns. The water loss and the volume shrinkage in the calcination process lead to the formation of pores [30]. Further, the nitrogen adsorption-desorption isotherms and the pore size distribution were measured, as shown in Fig. 4. Three isotherms can be categorized as type II with type H3 hysteresis loops, and the pore size distribution demonstrates that the pores are concentrated at ~3 nm, consistent with the TEM observations. The mesoporous structure can facilitate the electrolyte to saturate the active material [31], and thus improve the electrochemical performance [32]. The BET surface areas of the $NiCo_2O_4$/Ni foam electrodes with the morphologies of nanosheet, nanowire, and

nanoplate are measured to be 38.9, 51.8, and 45.8 m^2 g^{-1}, respectively; and the corresponding pore volumes are 0.068, 0.083, and 0.076 cm^3 g^{-1}, respectively. Thus, the $NiCo_2O_4$ electrode with the nanowire morphology has the largest specific surface area and pore volume, followed by the nanoplate, while the nanosheet $NiCo_2O_4$ electrode owns the lowest ones. The different geometrical properties of the electrodes will lead to different electrochemical performance in the battery.

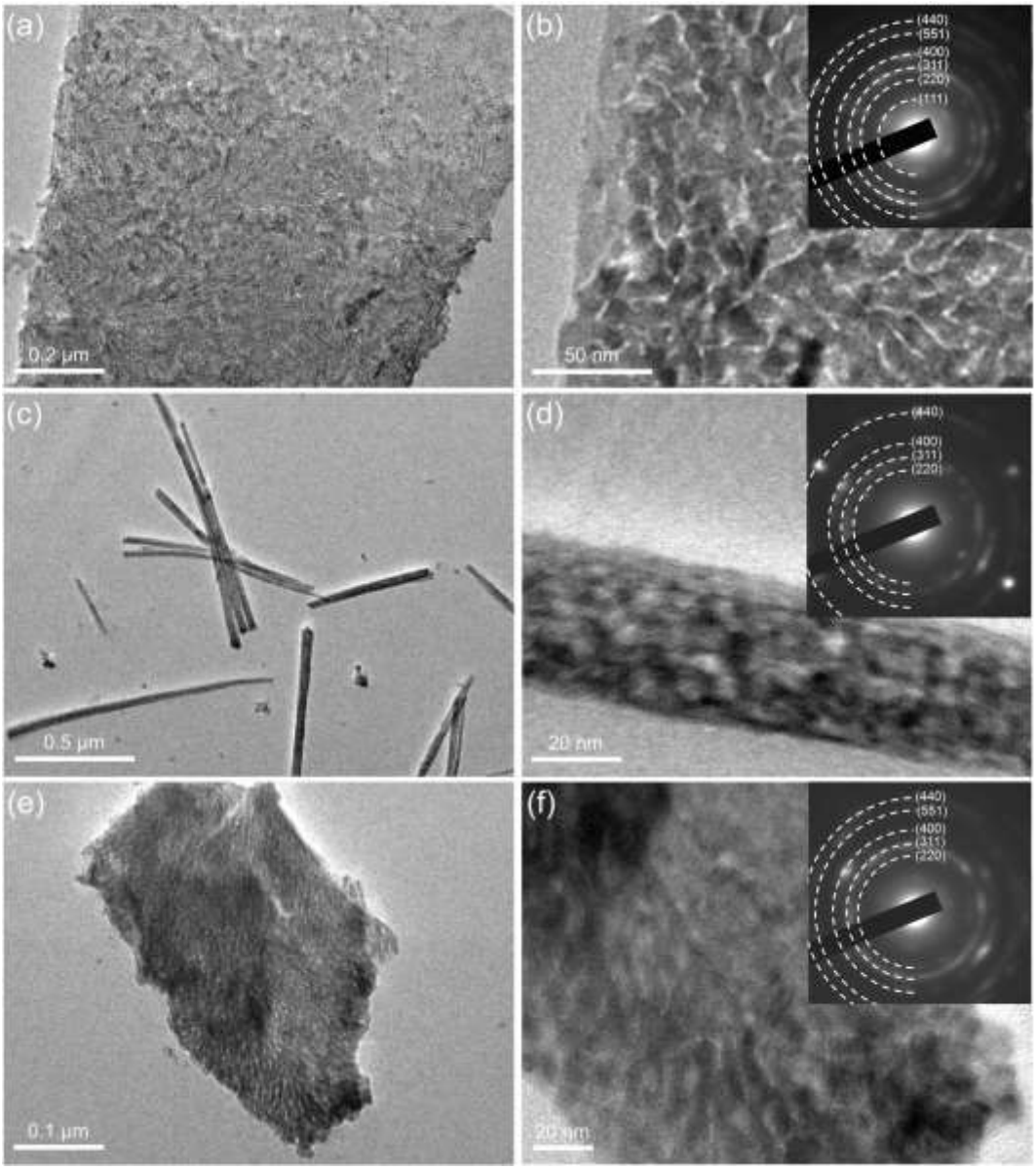

Fig. 3 TEM images of the nanostructured $NiCo_2O_4$ with different morphologies. (a-b) nanosheet, (c-d) nanowire, and (f-g) nanoplate. The insets show the corresponding

SAED patterns.

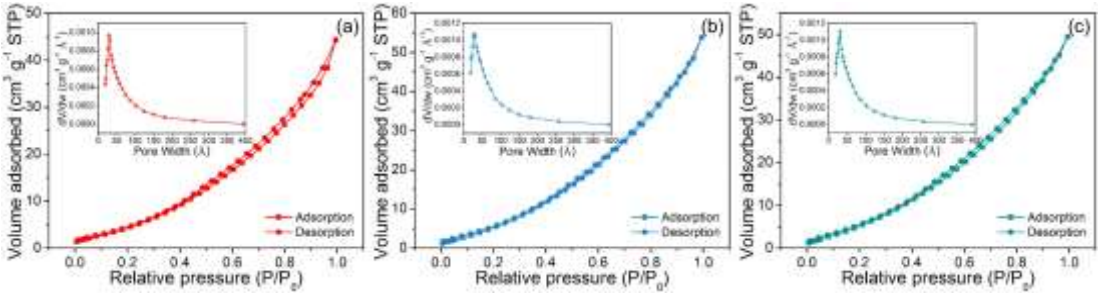

Fig. 4 Nitrogen adsorption-desorption isotherm of nanostructured $NiCo_2O_4$/Ni form. (a) nanosheet, (b) nanowire, and (c) nanoplate. The insets show the corresponding pore size distribution.

3.2 Electrochemical performance

Three Zn batteries assembled with the $NiCo_2O_4$ electrodes of different morphologies (nanosheet, nanowire, and nanoplate) were built to test the electrochemical performance. The reactions during the charge and discharge processes are proposed as follows [33]:

Positive electrode:

$$NiCo_2O_4 + OH^- + H_2O \underset{\text{charge}}{\overset{\text{discharge}}{\rightleftharpoons}} NiOOH + 2CoOOH + e^- \quad (1)$$

$$CoOOH + OH^- \underset{\text{charge}}{\overset{\text{discharge}}{\rightleftharpoons}} CoO_2 + H_2O + e^- \quad (2)$$

Negative electrode:

$$Zn(OH)_4^{2-} + 2e^- \underset{\text{charge}}{\overset{\text{discharge}}{\rightleftharpoons}} Zn + 4OH^- \quad (3)$$

Total reaction:

$$2NiCo_2O_4 + 3\left[Zn(OH)_4\right]^{2-} \underset{\text{charge}}{\overset{\text{discharge}}{\rightleftharpoons}} 3Zn + 2NiOOH + 4CoO_2 + 6OH^- + 2H_2O \quad (4)$$

During charge, $Zn(OH)_4^{2-}$ release OH^- into the electrolyte and turn into Zn at the negative electrode, while $NiCo_2O_4$ is transformed into NiOOH (NiO → NiOOH) and CoO_2 (Co_2O_3 → CoOOH → CoO_2) with OH^- from the electrolyte at the positive

electrode. During discharge, $Zn(OH)_4^{2-}$ is transformed into metallic Zn at the negative electrode, and the reduction of NiOOH and CoO_2 together with H_2O occurs to produce $NiCo_2O_4$ and OH^- at the positive electrode.

Fig. 5a presents the charge-discharge curves at the current densities of 0.5 A g^{-1} between 1.4 to 1.9 V. The batteries with the $NiCo_2O_4$ morphologies of nanosheet, nanowire, and nanoplate exhibit the average charge voltages of 1.80, 1.77, and 1.79 V, respectively, and deliver the average discharge voltage of ~1.7 V. The charge capacities are 135.17, 267.28, 183.31 mAh g^{-1}, respectively, and the discharge capacities are 109.9, 230.1, and 154.6 mAh g^{-1}, respectively. Thus, the coulombic efficiency of the battery is calculated to be 81.32%, 86.09%, and 84.34%, respectively; and the energy efficiency is 77.07%, 81.56%, and 79.55%, respectively.

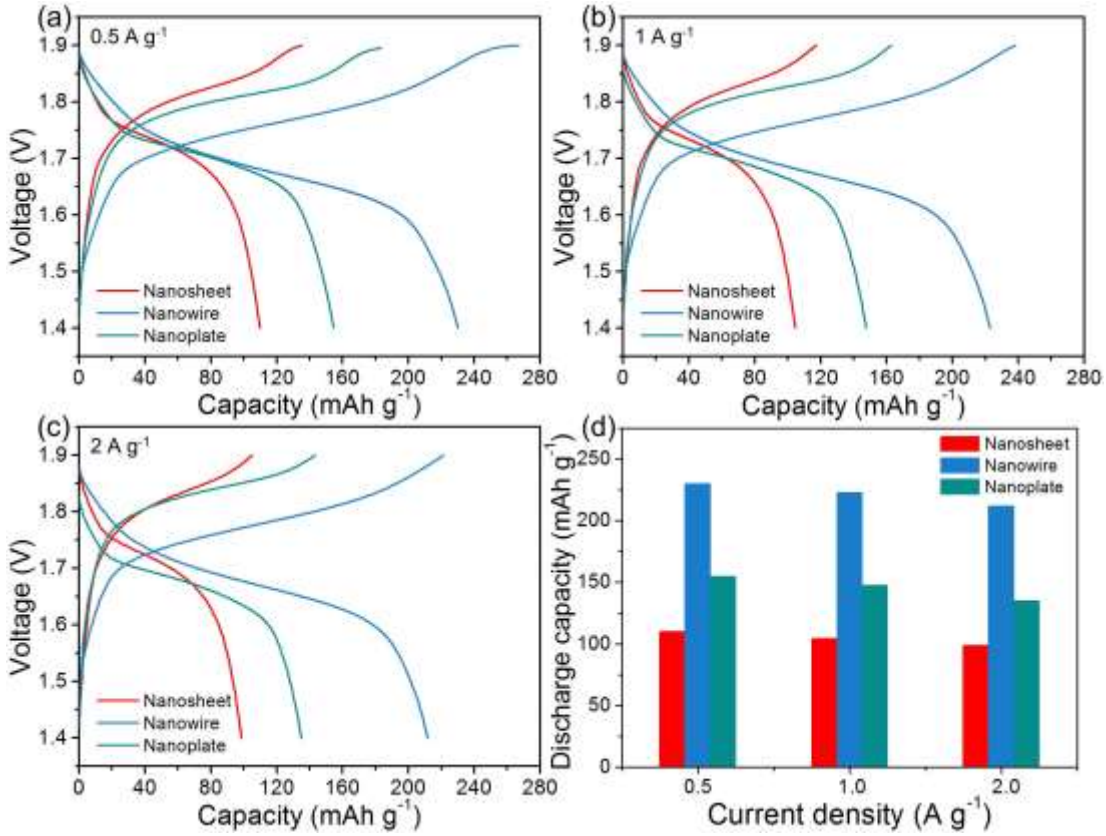

Fig. 5 Electrochemical performance of Zn batteries: (a-c) Voltage profiles of

nanostructured $NiCo_2O_4$ with different morphologies at the current density of (a) 0.5 A g^{-1}, (b) 1 A g^{-1}, and (c) 2 A g^{-1}. (d) Comparison of the discharge capacities at different current densities.

After charge, the $NiCo_2O_4$ electrodes were characterized by SEM. As displayed in Fig. S2, three electrodes preserved the initial morphologies, indicating the structural stability. To investigate the mechanisms during the charge process, the XPS characterization was carried out, and the results are shown in Fig. 6 and Table S1. For the Ni 2p spectra, the peaks at 854.2 and 871.8 eV are ascribed to Ni^{2+}, and at 855.7 and 873.4 eV are ascribed to Ni^{3+} [21]. For the pristine electrodes, the ratios of Ni^{2+}/Ni^{3+} in the morphologies of nanosheet, nanowire, and nanoplate are calculated to be 0.358, 0.484, and 0.264, respectively, indicating the mixed valence of Ni in $NiCo_2O_4$. After charge, the corresponding ratios become 0.063, 0.017, and 0.003, respectively. The small ratios indicate that the valence of Ni increases from +2 to +3, verifying the occurrence of Reaction 1 during charge. For the Co 2p spectra, the peaks at around 779.6 and 794.8 eV are ascribed to Co^{3+}, and other two peaks at around 781.5 and 796.4 eV are ascribed to Co^{4+} [34–36]. As listed in Table S2, the ratios of Co^{3+}/Co^{4+} before charge are 1.110, 0.963, and 0.859 for the electrodes with the morphologies of nanosheet, nanowire, and nanoplate, respectively, but decrease to 0.201, 0.403, and 0.402 after charge. The results demonstrate that the valences of partial Co atoms increase from +3 to +4 in $NiCo_2O_4$, verifying the occurrence of Reaction 2. In addition, compared with the results of Ni and Co, the utilization of Co ($Co^{3+} \rightarrow Co^{4+}$) seems to be less sufficient than that of Ni ($Ni^{2+} \rightarrow Ni^{3+}$), leading to

the difference between the practical (e.g., 230.1 mAh g^{-1}) and theoretical capacity (335 mAh g^{-1}) of $NiCo_2O_4$. Thus, further improving the utilization of Co is the key to enhance the capacity of the Zn-Co battery, which will be our future research topic.

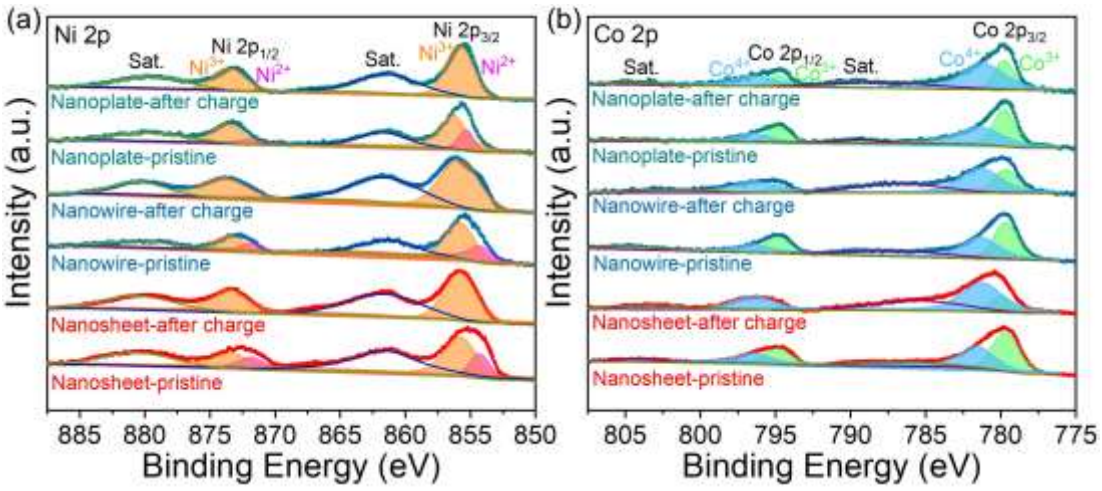

Fig. 6 XPS spectra of the nanostructured $NiCo_2O_4$ with different morphologies before and after charge: (a) Ni 2p and (b) Co 2p.

At the current densities of 1 and 2 A g^{-1} (Figs. 5b and 5c), the batteries deliver the similar discharge and charge performance to that at 0.5 A g^{-1}. Fig. 5d shows the comparison of the discharge capacities at different current densities. For the nanosheet electrode, when the current density increases from 0.5 to 1 and 2 A g^{-1}, the capacities are 109.9, 104.5, 98.6 mAh g^{-1}, respectively, with the retention rate of 89.7%. For the nanowire electrode, the capacities are 230.1, 222.7, and 211.7 mAh g^{-1}, respectively, with the retention rate of 92.0%. While the values of the nanoplate electrode are 147.6, 135.0, and 154.6 mAh g^{-1}, respectively, and the retention rate is 91.5%. Thus, the Zn battery with the $NiCo_2O_4$ nanowire electrode exhibits the best electrochemical performance, demonstrating that the capacity can be influenced by the morphology of the electrode material. It is worth noting that the discharge capacity reaches 230.1

mAh g^{-1} at 0.5 A g^{-1}, accounting for 68.7% of the theoretical capacity, higher than the reported Zn-Co battery with the Co_3O_4 nanowire electrode (38.9%) [10], demonstrating that the utilization of the active material can be effectively increased by the substitution of Ni and the morphology change. Based on the results above, the nanowire electrode performs excellently among three, which may be attributed to the high specific surface area, proper pore volume, and favorable nanostructure, greatly facilitating the species transport and the electrochemical reactions. Considering the average discharge voltage of ~1.7 V, the energy density achieved by the $NiCo_2O_4$ nanowire electrode is calculated to be 385.7 Wh kg^{-1}. When compared with the reported Co-based electrodes in alkaline electrolytes, as shown in Fig. 7, both the capacity and the energy density are superior [9,10,14,33,37], revealing the high performance of the $NiCo_2O_4$ nanowire electrode. Thus, this electrode was selected for in-depth studies in Zn batteries.

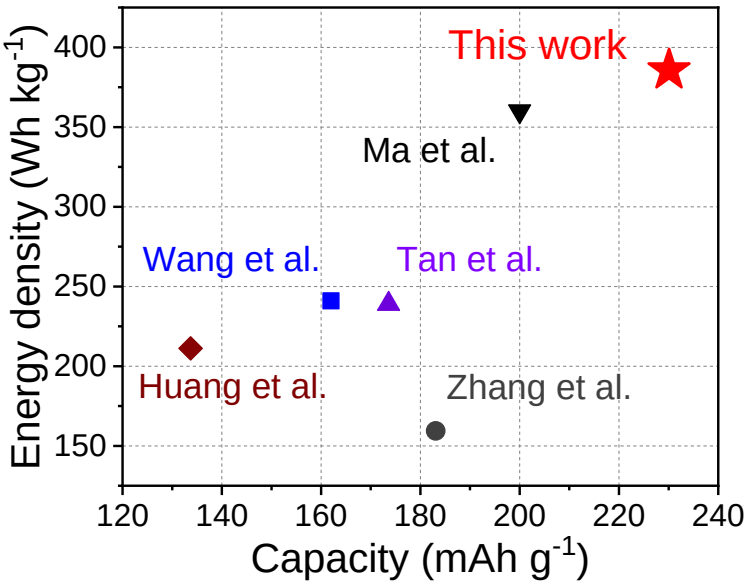

Fig. 7 Comparisons of the capacities and energy densities of Co-based electrode materials in alkaline-based Zn batteries.

The discharge and charge performance of the battery with the $NiCo_2O_4$ nanowire electrode at various current densities between the voltage of 1.4 to 1.9 V was tested, and the results are shown in Figs. 8a and 8b. When the current density increases from 0.5 to 1, 2, 4, 6 and 8 A g^{-1}, the average voltage gradually decreases from 1.68 to 1.63 V, and the capacity drops from 230.1 to 222.7, 211.7, 195.9, 180.4, and 164.3 mAh g^{-1}, respectively. Therefore, the coulombic efficiency of the battery is 86.09%, 93.45%, 95.63%, 95.92%, 96.86%, and 97.21%, respectively; and energy efficiency is 81.56%, 88.42%, 90.10%, 89.10%, 88.84%, and 88.13%, respectively. Thus, the capacity retention rate is calculated to be 71.4% when the current density changes from 0.5 to 8 A g^{-1}, demonstrating excellent rate performance [10].

To further evaluated the stability, the Zn battery with $NiCo_2O_4$ nanowire electrode was cycled at 8 A g^{-1}. As displayed in Fig. S3, initially, the coulomic efficiency and energy efficiency is 91.32%, and 86.60%, respectively; after 500 cycles, it shows 95.1% and 90.2%, respectively; while after 1000 cycles, the values are still close to 95.1% and 90.2%, respectively. However, with the cycle number increases, the discharge capacity decreases, which becomes 168.89 and 140.42 mAh g^{-1} at the 500^{th} and the 1000^{th} cycle, respectively. From Fig. 8c, after 1000 discharge and charge cycles, the battery can be operated normally and has the capacity retention of 63.23%, higher than some reported Zn batteries (e.g., Zn-NiO battery, ~65% after only 500 cycles) [19]. After the cycling test, we also examined the $NiCo_2O_4$ electrode, as shown in Fig. S4, both the morphology and the crystal structure remain well. Thus, this capacity loss may be mainly accounted for the instability of the Zn electrode,

which suffers from dendrite and passivation layers during cycling [38–41]. For this reason, tremendous efforts should also be devoted to solving the issues of Zn electrode to develop Zn batteries with better performance [42].

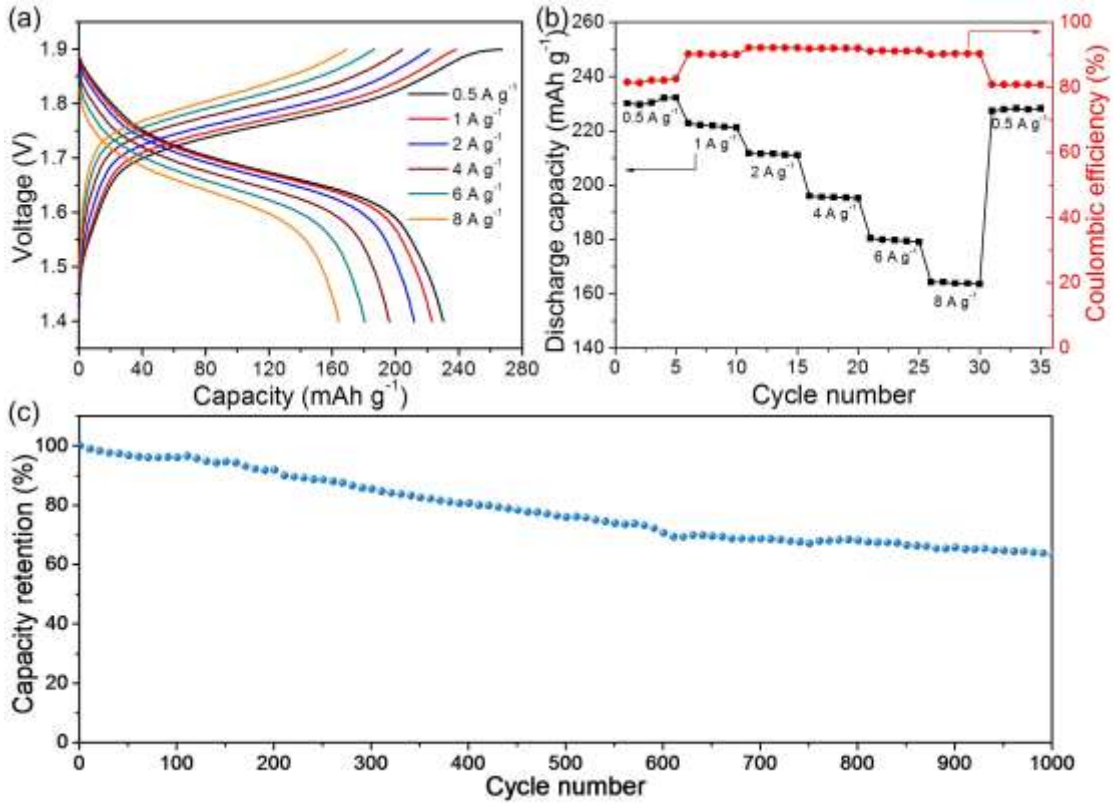

Fig. 8 Electrochemical performance of Zn batteries with the $NiCo_2O_4$ nanowire electrode: (a) voltage profile at different current densities, (b) summary of the discharge capacity and coulombic efficiency, and (c) capacity retention as a function of cycle number at 1 A g^{-1}.

4. Conclusions

In summary, a Zn battery based on $NiCo_2O_4$ as the positive material has been developed in this work. Nanostructured $NiCo_2O_4$ in-situ grown on the nickel foam substrate with different morphologies (nanosheet, nanowire, and nanoplate) is synthesized using hydrothermal methods, followed by calcination processes, which

exhibits hierarchical porous structure with a high specific surface area and proper pore volume. When assembled these electrodes in Zn batteries, at the current density of 0.5 A g^{-1}, the nanosheet, nanowire, and nanoplate electrodes deliver discharge capacities of 109.9, 230.1, and 154.6 mAh g^{-1}, respectively, and the energy densities research 187.15, 385.68, and 261.44 Wh kg^{-1}, respectively. Thus, the nanowire electrode exhibits the best electrochemical performance, especially the high utilization ratio of the active material (68.7%), evidently revealing the effectiveness in morphology control. Based on the weights of $NiCo_2O_4$ and consumed Zn, the energy density is calculated to be 301.3 Wh kg^{-1}, remarkably higher than those of reported Zn-Co batteries. Further, when the current density increases from 0.5 to 1, 2, 4, 6, 8 A g^{-1}, the battery with the $NiCo_2O_4$ nanowire electrode delivers the capacities of 230.1, 222.75, 211.72, 195.93, 180.38, and 164.25 mAh g^{-1}, respectively, with the capacity retention of 71.38%, demonstrating high rate performance. Moreover, the capacity retention is 63.23% after 1000 discharge-charge cycles. This work offers a promising positive electrode to achieve high-performance Zn batteries, and future research will focus on further improving the utilization of active materials and developing stable Zn electrodes.

Acknowledgments

P. Tan thanks the funding support from CAS Pioneer Hundred Talents Program. M. Ni thanks the funding support from The Hong Kong Polytechnic University (G-YBJN and G-YW2D), and a grant (Project Number: PolyU 152214/17E) from Research Grant Council, University Grants Committee, Hong Kong SAR.

References

[1] K. Xu, Nonaqueous liquid electrolytes for lithium-based rechargeable batteries, Chem. Rev. 104 (2004) 4303–4417.

[2] K. Kang, YS. Meng, J. Bréger, CP. Grey, G. Ceder, Electrodes with high power and high capacity for rechargeable lithium batteries, Science. 311 (2006), 977-980.

[3] N.S. Choi, Z. Chen, S.A. Freunberger, X. Ji, Y.K. Sun, K. Amine, G. Yushin, L.F. Nazar, J. Cho, P.G. Bruce, Challenges facing lithium batteries and electrical double-layer capacitors, Angew. Chemie. Int. Ed. 51 (2012) 9994–10024.

[4] L. Ji, M. Rao, S. Aloni, L. Wang, E.J. Cairns, Y. Zhang, Porous carbon nanofiber-sulfur composite electrodes for lithium/sulfur cells, Energy Environ. Sci. 4 (2011) 5053–5059.

[5] H. Kim, G. Jeong, Y.U. Kim, J.H. Kim, C.M. Park, H.J. Sohn, Metallic anodes for next generation secondary batteries, Chem. Soc. Rev. 42 (2013) 9011–9034.

[6] P. Tan, B. Chen, H. Xu, W. Cai, W. He, M. Liu, Z. Shao, M. Ni, Co3O4Nanosheets as Active Material for Hybrid Zn Batteries, Small. 14 (2018) 1–9.

[7] Y. Li, M. Gong, Y. Liang, J. Feng, J.E. Kim, H. Wang, G. Hong, B. Zhang, H. Dai, Advanced zinc-air batteries based on high-performance hybrid electrocatalysts, Nat. Commun. 4 (2013) 1805–1807.

[8] P. Tan, B. Chen, H. Xu, W. Cai, W. He, M. Ni, Investigation on the electrode design of hybrid Zn-Co_3O_4/air batteries for performance improvements,

Electrochim. Acta. 283 (2018) 1028–1036.

[9] L. Ma, S. Chen, H. Li, Z. Ruan, Z. Tang, Z. Liu, Z. Wang, Y. Huang, Z. Pei, J.A. Zapien, C. Zhi, Initiating a mild aqueous electrolyte Co_3O_4/Zn battery with 2.2 V-high voltage and 5000-cycle lifespan by a Co(iii) rich-electrode, Energy Environ. Sci. 11 (2018) 2521–2530.

[10] P. Tan, B. Chen, H. Xu, W. Cai, W. He, M. Ni, In-situ growth of Co_3O_4nanowire-assembled clusters on nickel foam for aqueous rechargeable Zn-Co_3O_4 and Zn-air batteries, Appl. Catal. B Environ. 241 (2019) 104–112.

[11] Y. Wu, Y. Zhang, Y. Ma, J.D. Howe, H. Yang, P. Chen, S. Aluri, N. Liu, Ion-Sieving Carbon Nanoshells for Deeply Rechargeable Zn-Based Aqueous Batteries, Adv. Energy Mater. 1802470 (2018) 1–7.

[12] W. Tang, Y. Hou, F. Wang, L. Liu, Y. Wu, K. Zhu, $LiMn_2O_4$ nanotube as cathode material of second-level charge capability for aqueous rechargeable batteries, Nano Lett. 13 (2013) 2036–2040.

[13] Rossen, A. What are metal prices like? Co-movement, price cycles and long-run trends. Resources Policy. 45 (2015) 255-276.

[14] X. Wang, F. Wang, L. Wang, M. Li, Y. Wang, B. Chen, Y. Zhu, L. Fu, L. Zha, L. Zhang, Y. Wu, W. Huang, An Aqueous Rechargeable Zn//Co_3O_4 Battery with High Energy Density and Good Cycling Behavior, Adv. Mater. 28 (2016) 4904–4911.

[15] J.K. Seo, J. Shin, H. Chung, P.Y. Meng, X. Wang, Y.S. Meng, Intercalation and conversion reactions of nanosized β-MnO_2 cathode in the secondary Zn/MnO_2

alkaline battery, J. Phys. Chem. C. 122 (2018) 11177–11185.

[16] P. Tan, B. Chen, H. Xu, W. Cai, M. Liu, Z. Shao, M. Ni, Nanoporous NiO/$Ni(OH)_2$ Plates Incorporated with Carbon Nanotubes as Active Materials of Rechargeable Hybrid Zinc Batteries for Improved Energy Efficiency and High-Rate Capability, J. Electrochem. Soc. 165 (2018) A2119–A2126.

[17] P. Tan, B. Chen, H. Xu, W. Cai, W. He, H. Zhang, M. Liu, Z. Shao, M. Ni, Integration of Zn-Ag and Zn-Air Batteries: A Hybrid Battery with the Advantages of Both, ACS Appl. Mater. Interfaces. 10 (2018) 36873–36881.

[18] A. Sobianowska-Turek, W. Szczepaniak, P. Maciejewski, M. Gawlik-Kobylińska, Recovery of zinc and manganese, and other metals (Fe, Cu, Ni, Co, Cd, Cr, Na, K) from Zn-MnO_2 and Zn-C waste batteries: Hydroxyl and carbonate co-precipitation from solution after reducing acidic leaching with use of oxalic acid, J. Power Sources. 325 (2016) 220–228.

[19] X. Wang, M. Li, Y. Wang, B. Chen, Y. Zhu, Y. Wu, A Zn-NiO rechargeable battery with long lifespan and high energy density, J. Mater. Chem. A. 3 (2015) 8280–8283.

[20] F. Wang, F. Yu, X. Wang, Z. Chang, L. Fu, Y. Zhu, Z. Wen, Y. Wu, W. Huang, Aqueous Rechargeable Zinc/Aluminum Ion Battery with Good Cycling Performance, ACS Appl. Mater. Interfaces. 8 (2016) 9022–9029.

[21] S. Liu, D. Ni, H.F. Li, K.N. Hui, C.Y. Ouyang, S.C. Jun, Effect of cation substitution on the pseudocapacitive performance of spinel cobaltite MCo_2O_4 (M = Mn, Ni, Cu, and Co), J. Mater. Chem. A. 6 (2018) 10674–10685.

[22] F. Cheng, J. Shen, B. Peng, Y. Pan, Z. Tao, J. Chen, of nanocrystalline spinels as oxygen reduction and evolution electrocatalysts, Nat. Chem. 3 (2010) 79–84.

[23] B. Chi, H. Lin, J. Li, Cations distribution of $Cu_xCo_{3-x}O_4$ and its electrocatalytic activities for oxygen evolution reaction, Int. J. Hydrogen Energ. 33 (2008) 4763–4768.

[24] T.W. Kim, M.A. Woo, M. Regis, K. Choi, Electrochemical Synthesis of Spinel Type $ZnCo_2O_4$ Electrodes for Use as Oxygen Evolution Reaction Catalysts, J. Phys. Chem. Lett. 5 (2014) 2–6.

[25] S. Singh, P. Pramanik, S. Sangaraju, A. Mallick, L. Giebeler, S. Thota, Size-dependent structural, magnetic, and optical properties of $MnCo_2O_4$ nanocrystallites, J. Appl. Phys. 121 (2017) 194303.

[26] Z. Yu, L. Chen, S. Yu, Growth of $NiFe_2O_4$ nanoparticles on carbon cloth for high performance flexible supercapacitors, J. Mater. Chem. (2014) 10889–10894.

[27] S. Liu, K.S. Hui, K.N. Hui, J.M. Yun, K.H. Kim, Vertically stacked bilayer $CuCo_2O_4$/$MnCo_2O_4$ heterostructures on functionalized graphite paper for high-performance electrochemical capacitors, J. Mater. Chem. A. (2016) 8061–8071.

[28] MCo_2O_4, T. S, Porous Nanorods as Bifunctional Cathode Materials for Lithium-O_2 Batteries Mohamed, Saad. Gomaa. (2015) 12038-12046.

[29] M. He, P. Zhang, S. Xu, X. Yan, Morphology Engineering of Co_3O_4 Nanoarrays As Free-Standing Catalysts for Lithium–Oxygen Batteries, ACS. Appl. Mater. Inter. 8 (2016) 23713-23720.

[30] Z. Zhu, J. Ping, X. Huang, J. Hu, Q. Chen, X. Ji, C.E. Banks, Hexagonal nickel oxide nanoplate-based electrochemical supercapacitor, J. Mater. Sci. 47 (2012) 503–507.

[31] P. Tan, M. Liu, Z. Shao, M. Ni, Recent Advances in Perovskite Oxides as Electrode Materials for Nonaqueous Lithium-Oxygen Batteries, Adv. Energy Mater. 7 (2017) 1602674.

[32] F. Cheng, J. Chen, Lithium-air batteries: Something from nothing, Nat. Chem. 4 (2012) 962–963.

[33] H. Zhang, X. Zhang, H. Li, Y. Zhang, Y. Zeng, Y. Tong, P. Zhang, X. Lu, Flexible rechargeable Ni//Zn battery based on self-supported $NiCo_2O_4$ nanosheets with high power density and good cycling stability, Green Energy Environ. 3 (2017) 56-62.

[34] J. Dupin, D. Gonbeau, H. Benqlilou-Moudden, P. Vinatier, A. Levasseur, XPS analysis of new lithium cobalt oxide thin-films before and after lithium deintercalation, Thin Solid Films. 384 (2001) 23–32.

[35] P. Liu, Z. Liu, P. Wu, X. Ou, Y. Zhang, W. Cai, F. Yu, M. Ni, S. Cheng, M. Liu, J. Liu, Enhanced capacitive performance of nickel oxide on porous $La_{0·7}Sr_{0·3}CoO_{3-\delta}$ ceramic substrate for electrochemical capacitors, Int. J. Hydrogen Energy. 43 (2018) 19589–19599.

[36] P. Liu, J. Liu, S. Cheng, W. Cai, F. Yu, Y. Zhang, P. Wu, M. Liu, A high-performance electrode for supercapacitors: Silver nanoparticles grown on a porous perovskite-type material $La_{0.7}Sr_{0.3}CoO_{3-\delta}$ substrate, Chem. Eng. J. 328

(2017) 1–10.

[37] H. Wang, J. Liu, J. Wang, M. Hu, Y. Feng, P. Wang, Y. Wang, N. Nie, J. Zhang, H. Chen, Q. Yuan, J. Wu, Y. Huang, Concentrated Hydrogel Electrolyte-Enabled Aqueous Rechargeable NiCo//Zn Battery Working from −20 to 50 °C, ACS Appl. Mater. Interfaces. (2018) DOI: 10.1021/acsami.8b18003.

[38] G. Fang, J. Zhou, A. Pan, S. Liang, Recent Advances in Aqueous Zinc-ion Batteries, ACS Energy Lett. 3 (2018), 2480-2501.

[39] D.U. Lee, J. Fu, M.G. Park, H. Liu, A. Ghorbani Kashkooli, Z. Chen, Self-Assembled NiO/$Ni(OH)_2$ Nanoflakes as Active Material for High-Power and High-Energy Hybrid Rechargeable Battery, Nano Lett. 16 (2016) 1794–1802.

[40] J. Fu, Z.P. Cano, M.G. Park, A. Yu, M. Fowler, Z. Chen, Electrically Rechargeable Zinc–Air Batteries: Progress, Challenges, and Perspectives, Adv. Mater. 29 (2017), 1604685.

[41] R. Ahmed, Durable High Surface Area Electrodes for Rechargeable Zinc Air Batteries, Master's thesis, University of Waterloo (2015).

[42] J.F. Parker, C.N. Chervin, I.R. Pala, M. Machler, M.F. Burz, J.W. Long, D.R. Rolison, Rechargeable nickel–3D zinc batteries: An energy-dense, safer alternative to lithium-ion, Science. 356 (2017) 415–418.